Supporting Information

Ultrathin Molybdenum Boride Films for Highly Efficient Catalysis of the Hydrogen Evolution Reaction

Xufeng Wang,[a,b]   Guoan Tai,[*a,b] Zenghui Wu,[a,b] Tingsong Hu,[a,b] and Rui Wang[a,b]

[a.] The State Key Laboratory of Mechanics and Control of Mechanical Structures, Laboratory of Intelligent Nano Materials and Devices of Ministry of Education, College of Aerospace Engineering, Nanjing University of Aeronautics and Astronautics, Nanjing 210016, China Address here.

[b.] School of Material Science and Technology, Nanjing University of Aeronautics and Astronautics, Nanjing 210016, China.

Corresponding author: taiguoan@nuaa.edu.cn

Table of Contents

1. Experimental Section

1.1 Synthesis and Transfer of Ultrathin Mo_3B Films

Typically, the boron source was prepared by mixing crystalline boron powders (99.99%) and boron oxide (B_2O_3) powders (99.98%) at a weight ratio of 1:1. Molybdenum (Mo) foil (99%, 20 μm) was selected as the substrate for synthesizing the ultrathin Mo_3B films. The powder mixture was loaded into a quartz boat. To grow Mo_3B ultrathin films, the powder mixture and the Mo foil with a size of 3×2 cm^2 were respectively placed in the source zone (T_1) and the deposition substrate zone (T_2) in a home-made two-zone chemical vapor deposition furnace. A cold trap was installed to prevent the damage of the scroll pump. The temperatures were separately controlled for the source zone (T_1 = 1100 ^oC) and the deposition zone (T_2 = 900 ^oC). Before the growth, the quartz tube was purged for 30 min with high-purity H_2 gas, and then a piece of Mo foil was annealed at 900 ^oC for 1 h to smooth the surface of the foils and enlarge the grain boundaries. Consequently, the temperature of the T_1 zone rose up to 1100 ^oC to produce a B_2O_2 vapor, which was transported by high-purity H_2 gas to the deposition zone to form ultrathin Mo_3B films on the Mo foil. In addition, MoO_2 and MoO_3 thin films on Mo foils have been grown under different temperature conditions at the same oxygen concentration. MoO_2 nanofilms on Mo foils was prepared at 1000 ^oC for 30 min while MoO_3 nanofilms on Mo foils was prepared at 600 ^oC for 30 min.

For transferring process, the protective layer PMMA was initially spin-coated onto one side of the sample and the other side of the sample was removed by mechanical grinding. The sacrificed Mo foil was dissolved after dipping into 2 M iron chloride ($FeCl_3$) acid. Then, the PMMA-Mo_3B films was transferred into 0.1 M diluted HCl for over 1 h in order to get rid of remaining metal flakes and dirties. Finally, the the PMMA-Mo_3B films was transferred onto SiO_2/Si substrate and the PMMA was removed by hot acetone at 80 ^oC.

1.2 Structural and Performance Characterization

The optical image of the boron films was characterized by optical microscopy (Olympus BX41). The morphology and energy dispersive X-ray spectroscopy (EDX) of the samples was performed on a Zeiss Merlin field emission scanning electron

microscopy (FESEM) instrument. Low-resolution and high-resolution TEM images and selected area electron diffraction (SAED) patterns were performed on a JEM 2100F system operated at 200 kV. Atomic force microscopy image was carried out using a SPI-3800N probe station controller in contact mode AFM, operating at room temperature. Electrochemical measurements were performed on a computer-controlled potentiostat (CHI660) using a saturated calomel electrode (SCE) as the reference. To compare the intrinsic HER activities of the samples, the cyclic voltammetry (CV) method was employed to measure the electrochemical double-layer capacitance (EDLC), C_{dl}.[1,2] The C_{dl} is expected to be linearly proportional to effective active surface area. The CV curves were measured at various scan rates at a potential range from -0.15 to 0 V vs the RHE region. The halves of the positive and negative current density differences $\Delta j/2$ ($\Delta j = j_a - j_c$) at the center of the scanning potential ranges are plotted *vs* the voltage scan rate.

2. Theoretical Calculation

2.1 Crystal Structure Analysis by Particle Swarm Optimization

The first principles calculations in the framework of density functional theory, including structural and electronic performances, was carried out based on the Cambridge Sequential Total Energy Package known as CASTEP.[3] The exchange–correlation functional under the generalized gradient approximation (GGA)[4] with norm-conserving pseudopotentials and Perdew–Burke–Ernzerhof functional was adopted to describe the electron–electron interaction.[5] An energy cutoff of 750 eV was used and a *k*-point sampling set of 4 x 4 x 2 for bulk and 4 x 4 x 1 for surface were tested to be converged. Each atom in the storage models is allowed to relax to the minimum in the enthalpy without any constraints. The vacuum space along the *z* direction is set to be 15 Å, which is enough to avoid interaction between the two neighboring images. A force tolerance of 0.01 eV Å^{-1}, energy tolerance of 1.0×10^{-5} eV per atom and maximum displacement of 1.0×10^{-3} Å were considered.

2.2 Free Energy Calculations for Hydrogen Adsorption

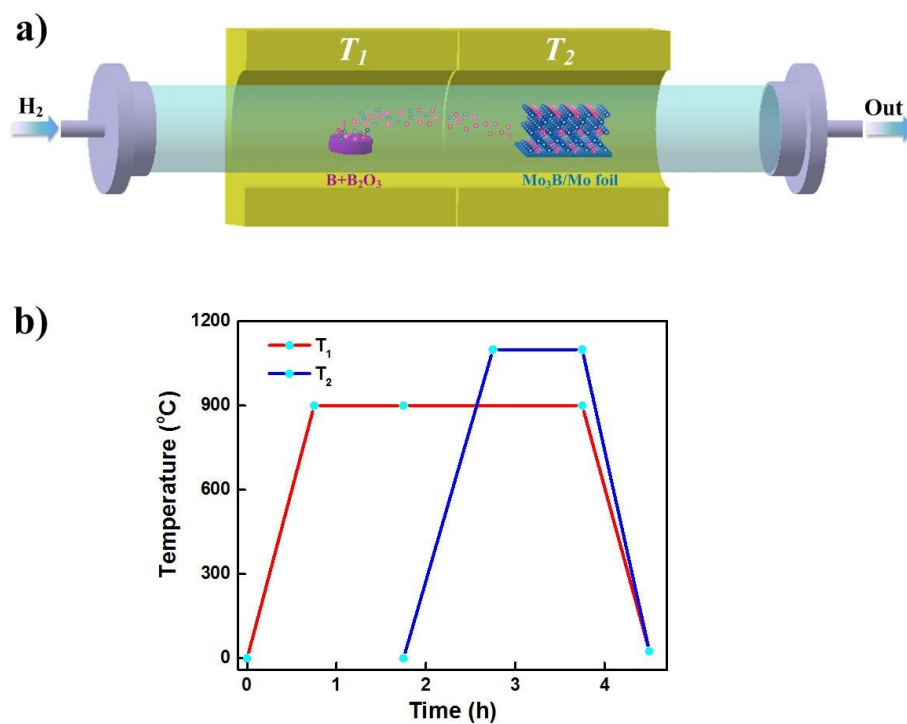H adsorption energies were calculated relative to H_2 (g) as:

$$\Delta E = E(\text{slab+H}) - E(\text{slab}) - \tfrac{1}{2}E(\text{H}_2) \tag{1}$$

The associated free energy of H is

$$\Delta G = \Delta E + \Delta ZPE - T\Delta S \tag{2}$$

where ΔZPE being the difference in zero-point energy and ΔS the difference in entropy between the adsorbed state and gas phase. Since $\Delta ZPE - T\Delta S \approx 0.28$ eV,[6] we have $\Delta G = \Delta E + 0.28$ eV.

Figures S1-S13

Figure S1. Experimental setup of synthesizing ultrathin Mo_3B films. (a) Schematic illustration of fabricating ultrathin Mo_3B films. (b) Temperature profile of the source zone (T_1) and the deposition zone (T_2).
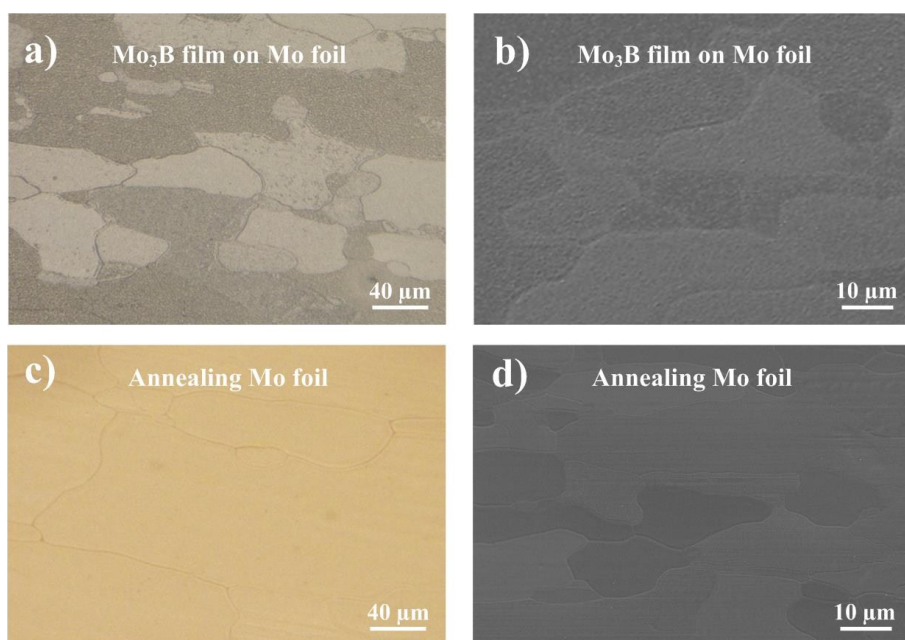
Figure S2. Structural characterization of ultrathin Mo$_3$B films. (a,b) Optical and SEM images of as-synthesized ultrathin Mo$_3$B films on Mo foils. (c,d) Optical and scanning electron microscopy (SEM) images of annealed Mo foils at 1400 ^{o}C for 10 h.
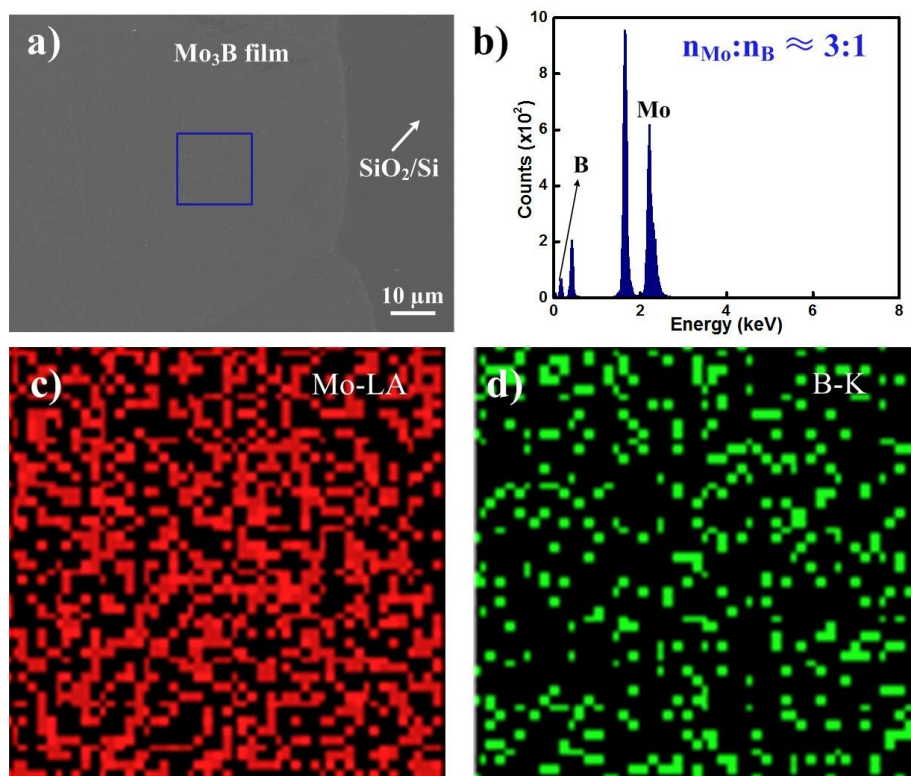
Figure S3. Structural and energy X-ray spectroscopy characterization of ultrathin Mo_3B films. (a) SEM image of the ultrathin Mo_3B film on a 285-nm SiO_2/Si substrate. (b) Energy dispersive X-ray spectroscopy (EDX) of the ultrathin Mo_3B film on a 285-nm SiO_2/Si substrate. (c) Molybdenum elemental mapping in the sample. (d) Boron elemental mapping in the sample.
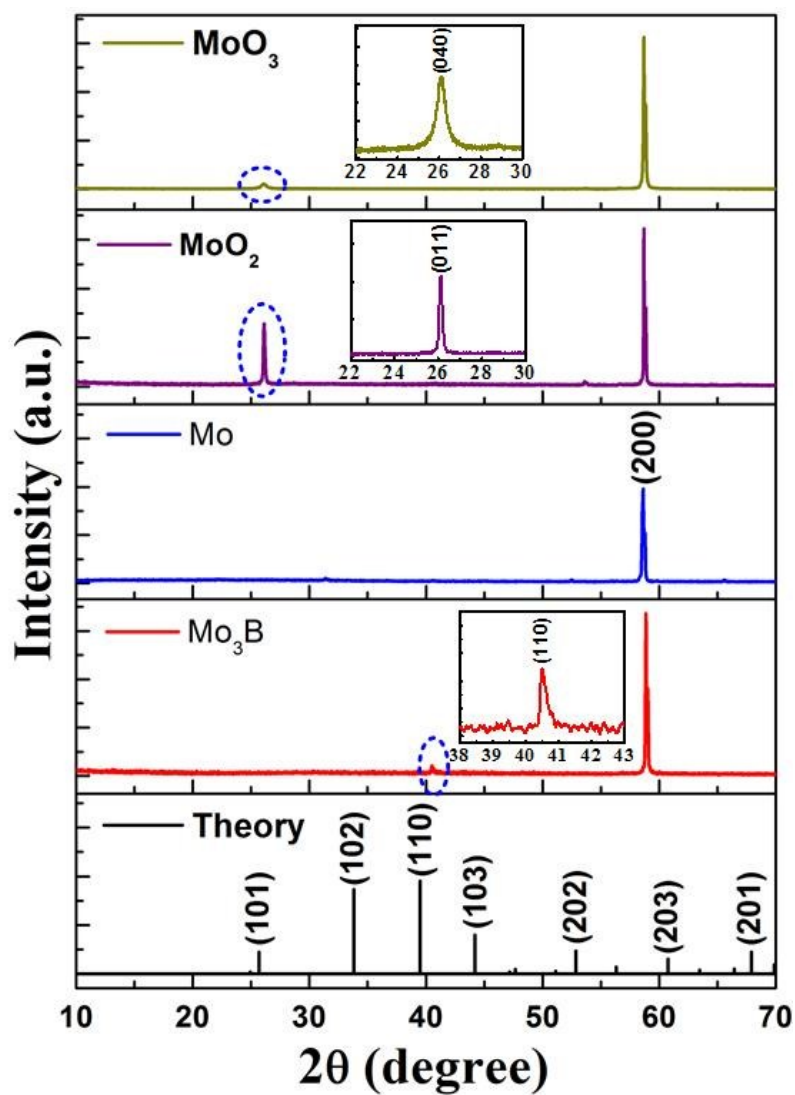
Figure S4. Grazing angle incidence XRD patterns of ultrathin Mo_3B film, Mo foil, MoO_2 and MoO_3 thin films. The (040) diffraction peak can be indexed to MoO_3 (JCPDS No. 35-0609), the (011) diffraction peak can be indexed to MoO_2 (JCPDS No. 65-1273) and the (200) diffraction peak can be indexed to Mo (JCPDS No. 89-5023).
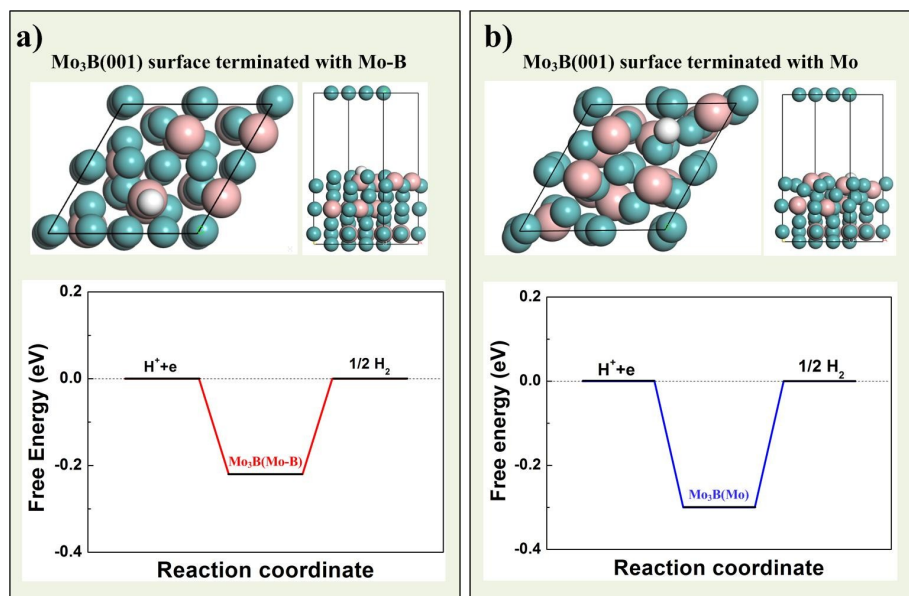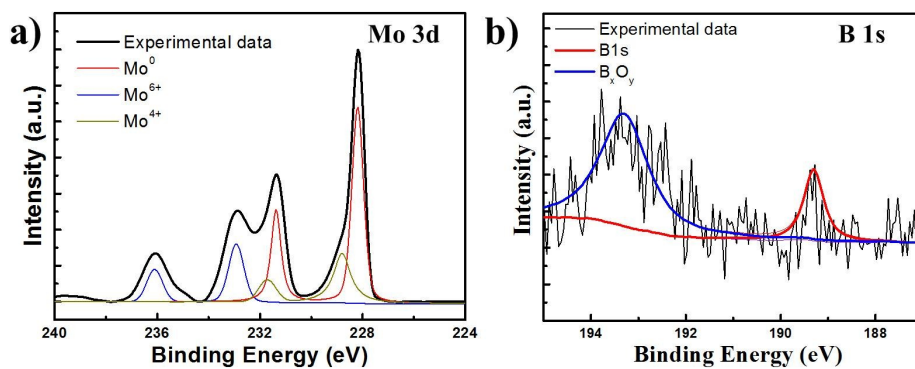
Figure S5. Structure diagram of $Mo_3B(001)$ surface terminated with Mo-B and Mo. (a) The structure and free energy diagram of $Mo_3B(001)$ surface terminated with Mo-B. (b) The structure and free energy diagram of $Mo_3B(001)$ surface terminated with Mo.
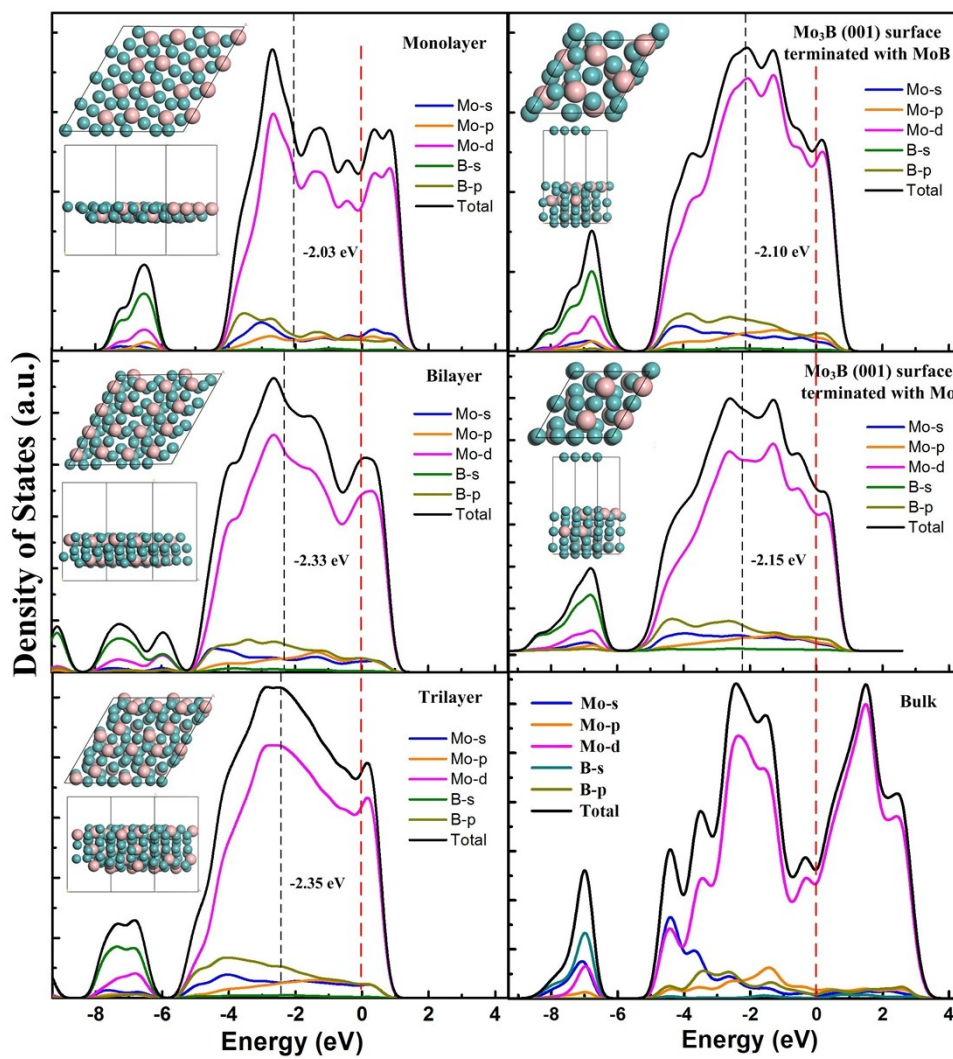
**Figure S6.** DOS patterns of mono-, bi- and trilayer Mo$_3$B, its surface terminated Mo-B and Mo as well as the bulk counterpart.

Figure S7. X-ray photoelectron spectra (XPS) patterns of ultrathin Mo_3B film. (a) XPS pattern of Mo 3d in the ultrathin Mo_3B film. Experimental data (black curve), MoO_3 (Mo^{6+}), MoO_2 (Mo^{4+}) and Mo (Mo^0) peaks from the boride thin film. (b) XPS pattern of B 1s in the ultrathin Mo_3B film.
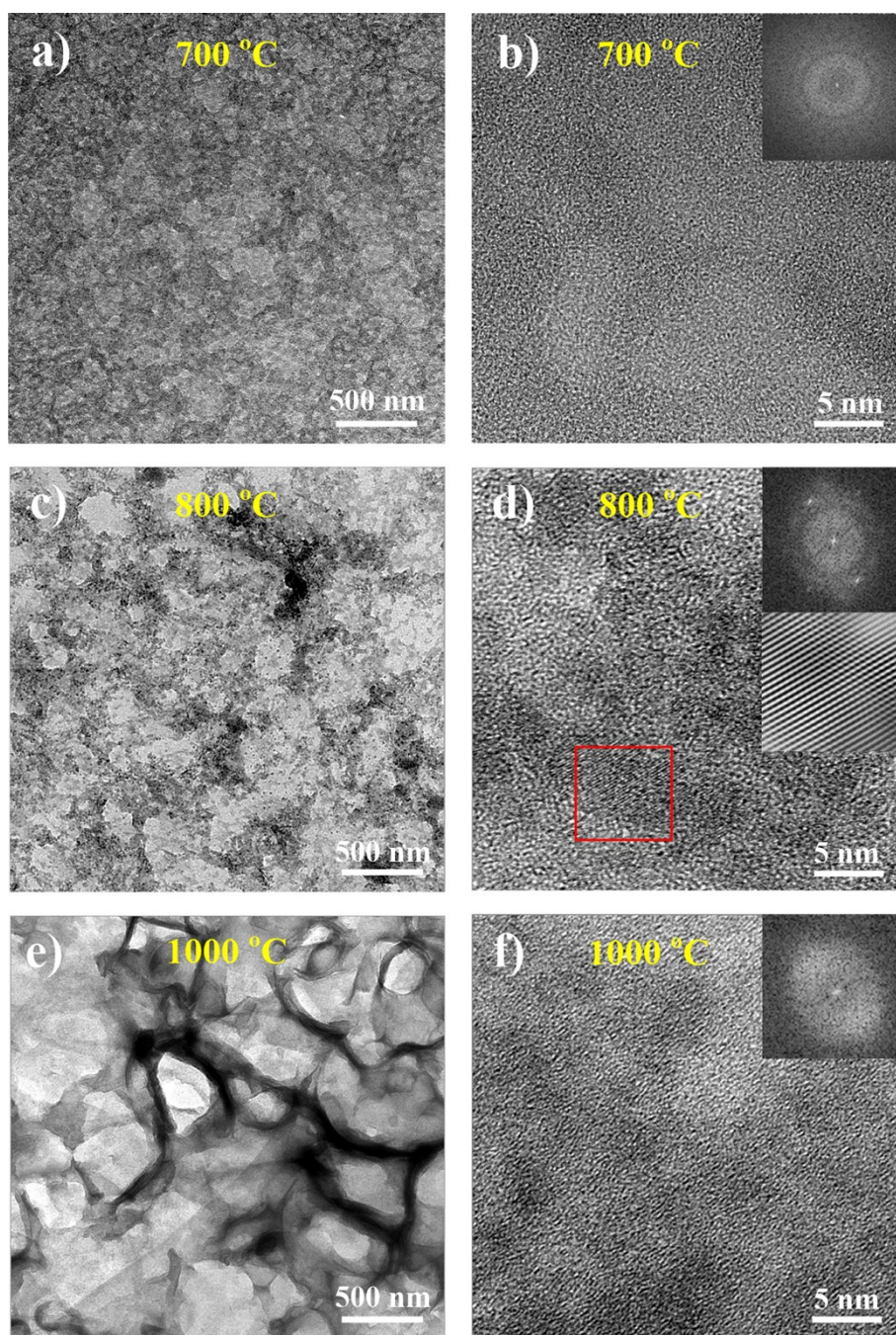
Figure S8. TEM and HRTEM images of the samples grown at different temperatures: (a,b) 700, (c,d) 800 and (e,f) 1000 °C. The corresponding fast Fourier transform (FFT) patterns are inserted into the upper right of (b), (d) and (f).
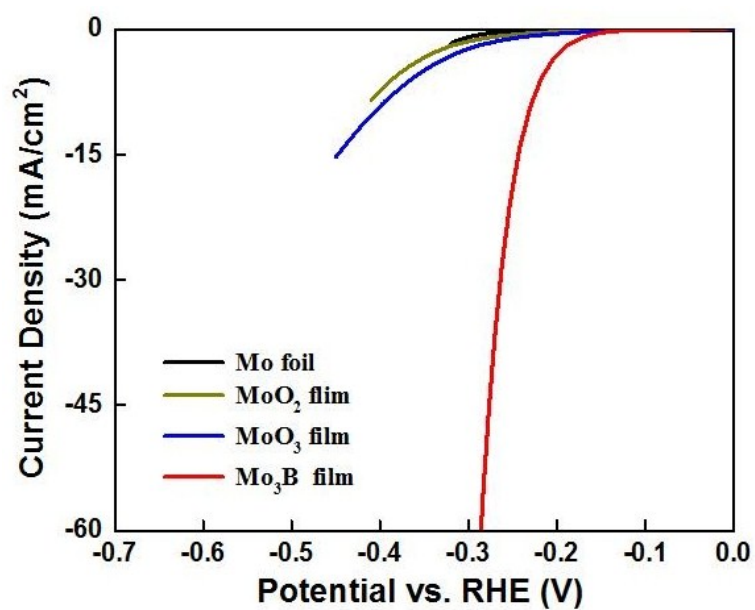
Figure S9. HER *iR*-corrected LSV curves of ultrathin Mo_3B films on the Mo foil in 0.5 M H_2SO_4, along with a pure Mo foil, MoO_2 and MoO_3 film on Mo foils. The scanning rate is 5 mV/s.
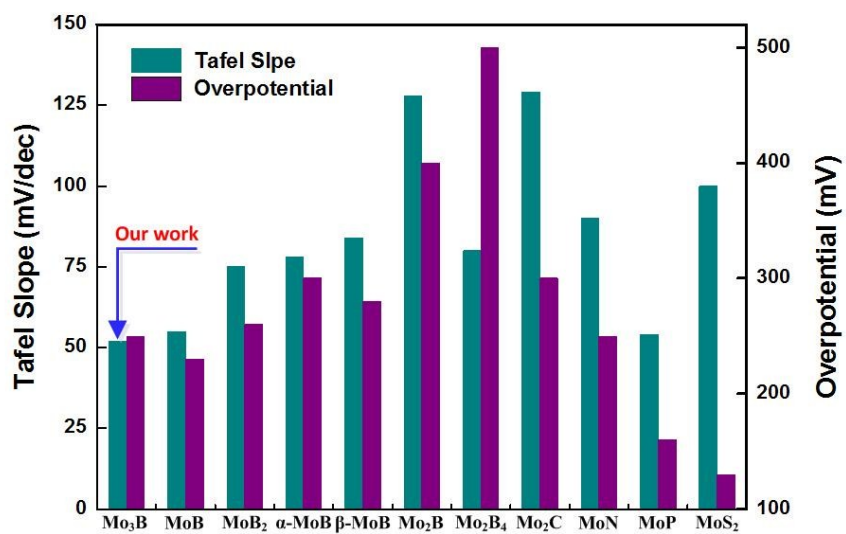
**Figure S10.** Tafel slope and overpotential analysis of different HER catalysts in acid solutions.
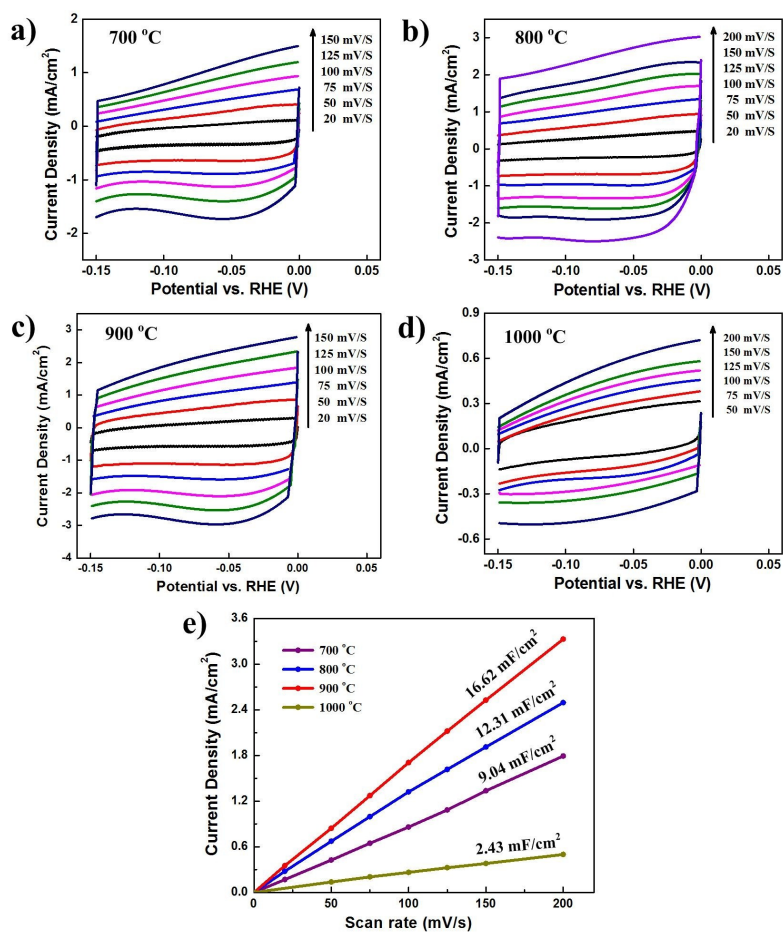
Figure S11. CV curves of ultrathin Mo_3B films. (a-d) CV curves at various scan rates to determine the C_{dl} values of the thin films obtained at different reaction temperatures: (a) 700, (b) 800, (c) 900 and (d) 1000 °C. (e) The capacitive current density as a function of scan rate.
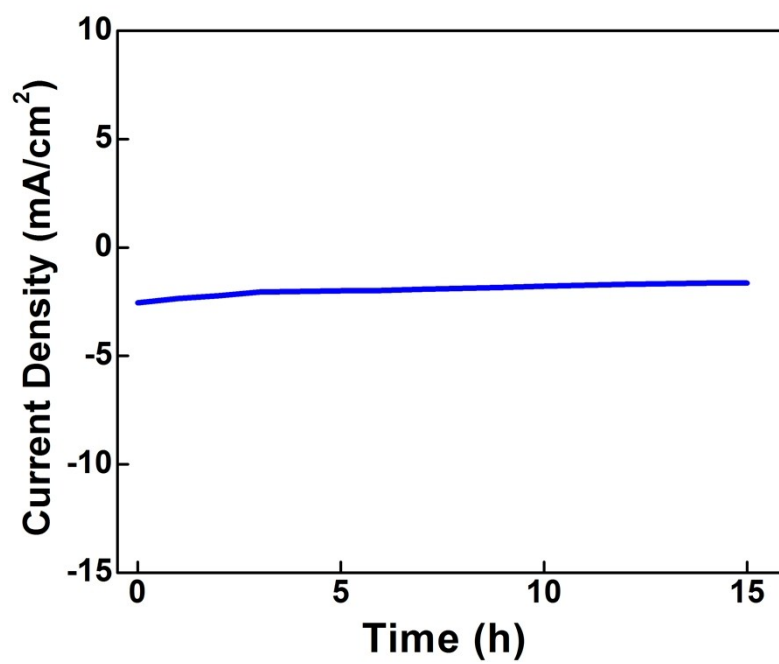
Figure S12. Durability of the ultrathin Mo$_3$B film at a constant overpotential of 200 mV for 15 h.
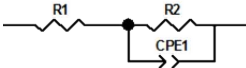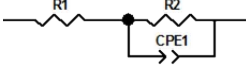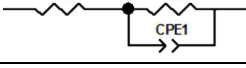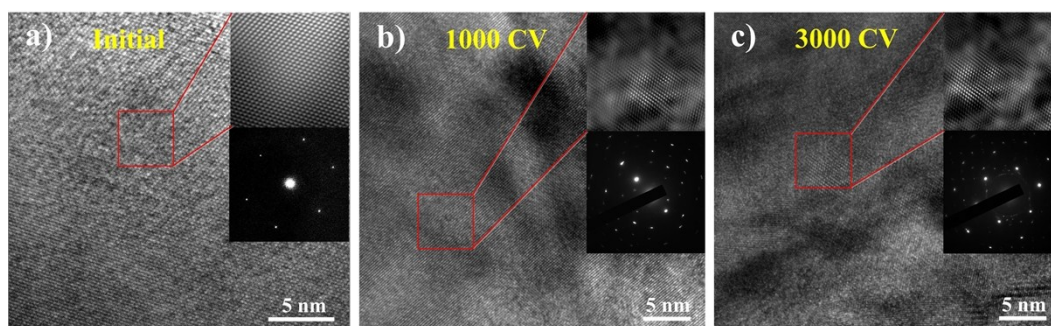
Figure S13. HRTEM images of the sample: (a) initial, (b) after 1000 CV sweeps and (c) after 3000 CV sweeps.

Table S1. Summary of the reported Mo-based catalysts in 0.5 M H_2SO_4 solution

Catalyst	Overpotential (mV) at 20mA/cm^2	Tafel slope (mV/dec)	References
Mo$_3$B film	**249**	**52**	**Our work**
MoB particles	230	55	[7]
MoB$_2$ powders	> 260	75	[8]
α-MoB powders	> 300	78	[8]
β-MoB powders	> 280	84	[8]
Mo$_2$B powders	> 300	128	[8]
Mo$_2$B$_4$ powders	>500	80	[9]
Mo$_2$C particles	230	56	[10]
MoN film	250	90	[11]
MoP Nanoparticles	160	54	[12]
MoS$_2$ film	130	100	[13]

Table S2. The equivalent circuit diagram and corresponding R_1 and R_2 values at different temperatures

Sample	Equivalent circuit diagram	R_1 (R_s)	R_2 (R_{ct})
S-700		2.808	10923
S-800		2.843	9446
S-900		2.939	**5415**
S-1000		2.214	10452
Mo foil		1.417	29176

Note: 1) R_s is resistance of the electrolyte, R_{ct} is charge transfer resistance and *CPE* is constant phase element.

2) S-700, S-800, S-900 and S-1000 refer to the samples grown at different temperatures of 700, 800, 900 and 1000 ℃, respectively.

References

(1) J. D. Benck, T. R. Hellstern, J. Kibsgaard, P. Chakthranont and T. F. Jaramillo, *ACS Catal.*, 2014, **4**, 3957 – 3971.

(2) C. Q. Sun, J. Y. Zhang, J. Ma, P. T. Liu, D. Q. Gao, K. Tao and D. S. Xue, *J. Mater. Chem. A*, 2016, **4**, 11234 – 11238.

(3) M. D. Segall, P. J. D. L. M. J. Probert, C. J. Pickard, P. J. Hasnip, S. J. Clark and M. C. Payne, *J. Phys.*: *Condens. Matter.*, 2002, **14**, 2717 – 2744.

(4) J. P. Perdew, K. Burke and M. Ernzerhof, *Phys. Rev. Lett.*, 1996, **77**, 3865.

(5) D. R. Hamann, M. Schluter and C. Chiang, *Phys. Rev. Lett.*, 1979, **43**, 1494.

(6) D. Voiry, H. Yamaguchi, J. Li, R. Silva, D. C. Alves, T. Fujita, M. Chen, T. Asefa, V. B. Shenoy, G. Eda and M. Chhowalla, *Nat. Mater.*, 2013, **12**, 850 – 855.

(7) H. Vrubel and X. L. Hu, *Angew. Chem. Int. Ed.*, 2012, **51**, 12703 – 12706; *Angew. Chem.*, 2012, **124**, 12875 – 12878.

(8) H. Park, A. Encinas, J. P. Scheifers, Y. Zhang and B. P. T. Fokwa, *Angew. Chem. Int. Ed.*, 2017, **56**, 5575 – 5578; *Angew. Chem.*, 2017, **129**, 5667 – 5670.

(9) H. Park, Y. Zhang, J. P. Scheifers, P. R. Jothi, A. Encinas and B. P. T. Fokwa, *J. Am. Chem. Soc.*, 2017, **139**, 12915 – 12918.

(10) X. Fan, Y. Liu, Z. Peng, Z. Zhang, H. Zhou, X. Zhang, B. I. Yakobson, W. A. Goddard, X. Guo, R. H. Hauge and J. M. Tour, *ACS Nano*, 2017, **11**, 384 – 394.

(11) J. Xie, S. Li, X. Zhang, J. Zhang, R. Wang, H. Zhang, B. Pan and Y. Xie, *Chem. Sci.*, 2014, **5**, 4615.

(12) P. Xiao, M. A. Sk, L. Thia, X. Ge, R. J. Lim, J.-Y. Wang, K. H. Lima and X. Wang, *Energy Environ. Sci.*, 2014, **7**, 2624 – 2629.

(13) L. Yang, W. Zhou, D. Hou, K. Zhou, G. Li, Z. Tang, L. Li and S. Chen, *Nanoscale*, 2015, **7**, 5203 – 5208.